Influence of oblique wave attack on wave overtopping at caisson breakwaters with sea and swell conditions

van Gent, Marcel R.A.

DOI
10.1016/j.coastaleng.2020.103834

Publication date
2021

Document Version
Final published version

Published in
Coastal Engineering

Citation (APA)
van Gent, M. R. A. (2021). Influence of oblique wave attack on wave overtopping at caisson breakwaters with sea and swell conditions. *Coastal Engineering*, *164*, 1-15. Article 103834. https://doi.org/10.1016/j.coastaleng.2020.103834

Coastal Engineering 164 (2021) 103834

Contents lists available at ScienceDirect

Coastal Engineering

journal homepage: http://www.elsevier.com/locate/coastaleng

Influence of oblique wave attack on wave overtopping at caisson breakwaters with sea and swell conditions

Marcel R.A. van Gent [a,b,*]

[a] Dept. Coastal Structures & Waves, Deltares, Delft, the Netherlands
[b] Dept. Hydraulic Engineering, TU Delft, the Netherlands

ARTICLE INFO

Keywords:
Wave overtopping
Oblique waves
Angle of wave attack
Caisson breakwater
Vertical breakwater
Recurved parapet
Bullnose
Bimodal wave conditions
Crossing seas
Physical model tests
Wave basin
Corner section
Design guidelines

ABSTRACT

The amount of wave overtopping at coastal structures such as vertical caisson breakwaters is strongly dependent on the angle of wave attack. The reducing effects of oblique waves on wave overtopping compared to perpendicular wave attack has been studied by means of three-dimensional wave basin tests. In these physical model tests the caisson breakwater has been exposed to wave conditions with wave angles between perpendicular and very oblique waves (*i.e.* 0°–75° in steps of 15°). Short-crested and long-crested waves have been tested and analysed. Also, crossing bimodal conditions have been studied with directional wind waves approaching the breakwater under a different angle than the simultaneous unidirectional swell conditions. Vertical caisson breakwaters with and without a recurved parapet (also referred to as a bullnose or a recurved wave return wall) have been tested. The measurements showed the large influence of oblique waves on wave overtopping. Also, the influence of a recurved parapet can be large although the influence reduces for larger wave angles. Guidelines have been proposed to account for the influence of oblique waves on wave overtopping at vertical caisson breakwaters with and without a recurved parapet, as well as for crossing bimodal conditions with simultaneous sea and swell conditions from different directions.

1. Introduction

Severe wave overtopping at vertical caisson breakwaters and seawalls may cause a threat to people, accessibility, infrastructure and equipment at the crest and landside of the breakwater. Therefore, the crest level of vertical caisson breakwaters and seawalls is often based on estimates of the wave overtopping during storms. Wave overtopping is affected by the water levels, the wave loading, and the geometry of the structure. One of the important effects of the wave loading is the angle between the waves and the structure. Perpendicular wave loading leads to the largest amount of wave overtopping. However, in many circumstances the wave direction of the dominant waves is not perpendicular. In order to assess the required crest level for vertical breakwaters and seawalls under oblique wave attack, information is required on the reduction of wave overtopping due to the angle between the waves and the structure.

For vertical caisson breakwaters (examples are shown in Fig. 1) limited data are available to estimate the reducing effects of oblique waves. Therefore, new physical model tests in a wave basin with oblique waves have been performed for three types of wave loading: (a) Short-crested waves with a pre-defined amount of directional spreading, (b) Long-crested (unidirectional) waves, and (c) Bimodal crossing wave conditions that consist of (short-crested) wind waves from one mean wave direction in combination with simultaneous (unidirectional) swell waves from another wave direction.

To reduce wave overtopping at vertical caisson breakwaters or at the crest wall at the top of a rubble mound breakwater, often use is made of a recurved parapet at the top of the seaward side of the front wall. Adding recurved parapets on top of existing caisson breakwaters can be a solution to adapt existing caisson breakwaters to account for effects of sea level rise. Fig. 1 (lower-mid and lower-right) show examples of a recurved parapet, also referred to as a bullnose or a recurved wave return wall. The influence of oblique waves is potentially affected by the presence of a recurved parapet, and therefore this aspect of oblique waves has been studied here for vertical caisson breakwaters with and without a recurved parapet.

The structure of the paper is as follows. First a selection of literature for caisson breakwaters is discussed in Section 2. In Section 3 the new physical model tests are presented. In Section 4 the analysis of the data and new guidelines to account for oblique waves for vertical caisson

* Dept. Coastal Structures & Waves, Deltares, Delft, the Netherlands.
E-mail address: Marcel.vanGent@deltares.nl.

https://doi.org/10.1016/j.coastaleng.2020.103834
Received 14 October 2020; Received in revised form 7 December 2020; Accepted 12 December 2020
Available online 23 December 2020

breakwaters, are presented. Finally, conclusions are drawn, and recommendations are provided.

2. Wave overtopping at caisson breakwaters

For the design of caisson breakwaters not only the amount of wave overtopping is relevant, but also their stability with respect to horizontal forces and vertical uplift forces. For some caisson structures inside a port, or close to a harbour approach channel, the wave reflection by vertical caisson breakwaters plays a role. To reduce wave reflection by the vertical caisson breakwater and to reduce the forces on the front wall, the front wall can be constructed as a perforated wall with one or multiple energy dissipation chambers inside the caisson. The present research is focussed on unperforated caisson breakwaters.

2.1. Forces on caisson breakwaters

In the design of caisson breakwaters often configurations are selected that do not lead to high impulsive wave forces since impulsive wave forces are generally significantly larger than the so-called non-impulsive wave forces. For instance, a rubble mound berm in front of a caisson breakwater often leads to impulsive wave forces and therefore a berm in front of a caisson breakwater is generally omitted. Since configurations leading to impulsive wave loads on the caissons itself are generally omitted, the present research on wave overtopping is focussed on caisson breakwaters that do not lead to impulsive wave loads on the caisson itself. Based on E.A. manual (1999), non-impulsive loading is expected if $(h/H_{m0})^2 s_{m\text{-}1,0} > 0.25$ where H_{m0} is the spectral significant wave height of the incident waves at the toe of the structure H_s=H_{m0} (m), h is the water depth in front of the structure (m) and $s_{m\text{-}1,0}$ is the wave steepness ($s_{m\text{-}1,0} = 2\pi H_{m0}/gT^2_{m\text{-}1,0}$ where $T_{m\text{-}1,0}$ is the spectral mean wave period).

To assess forces on caisson breakwaters several methods are available. Guidelines and valuable information to estimate horizontal forces and vertical uplift forces are available, e.g. Goda (1974, 1985, 2010), Takahashi (1996), Tabet-Aoul and Lambert (1998) and Franco et al. (1998). Physical model tests are generally accepted as the most accurate way to obtain estimates of forces on specific caisson breakwaters with conditions and configurations that have not been tested before. Based on available data from physical model tests also data-driven methods can be used to obtain estimates within the ranges of the relevant parameters of the data. See for instance Van Gent and van den Boogaard (1998) for the description of an Artificial Neural Network to obtain estimates of the forces on caisson breakwaters. Estimates of forces on caisson breakwaters can also be obtained by performing numerical model computations, see for instance Takahashi et al. (2002) and Castellino et al. (2018). To reduce wave overtopping a recurved parapet can be applied. Castellino et al. (2018) and Martinelli et al. (2018) studied the forces on recurved parapets. It was shown that impulsive wave loads can occur on recurved parapets, also for cases with non-impulsive wave loads on the front face of the caisson breakwater.

2.2. Wave overtopping predictions

After the pioneering research with respect to wave overtopping by Goda (1971), Battjes (1974) and Owen (1980), various formulae have been developed to predict wave overtopping at caisson breakwaters. Many of these formulae can be rewritten as follows:

$$\frac{q}{\sqrt{gH_{m0}^3}} = a \exp\left[-\frac{b}{\gamma}\left(\frac{R_c}{H_{m0}}\right)^c\right] \quad (1)$$

Fig. 1. Vertical caisson breakwater under construction (upper panel), corner section (lower-left panel), and recurved parapets (lower-mid and lower-right panels; courtesy M. Castellino).

where q is the mean wave overtopping discharge ($m^3/s/m$), g is the acceleration due to gravity (m/s^2), R_c is the crest height (including the height of a parapet, if present) relative to the still water level (m), H_{m0} is the spectral significant wave height of the incident waves at the toe of the structure H_s=H_{m0} (m), γ denotes the influence factor for effects such as the influence of the angle of wave attack (γ_β) and/or the influence of a recurved parapet (γ_p) and b and c are coefficients. Note that $Q = q/(gH_{m0}^3)^{0.5}$ is the non-dimensional wave overtopping discharge. Eq. (1) will be applied and discussed more in detail in the section describing the analysis of the test results.

Based on available data from physical model tests also data-driven methods can be used to obtain estimates of wave overtopping discharges for conditions within the ranges of the relevant parameters of the data. See for instance Van Gent et al. (2007) and Den Bieman et al. (2020) for data-driven methods to estimate wave overtopping at coastal structures including caisson breakwaters. Within parameter ranges that are well covered by the data, these methods generally outperform empirical expressions but the dependency of wave overtopping on the most important parameters is less clearly visible than expressed in empirical expressions.

2.3. Shallow water

Often caisson breakwaters are more economical for relatively deep-water conditions while rubble mound breakwaters are often more economical for shallow water conditions. Therefore, the present tests are focussed on conditions with relatively deep water at the toe, thus without important wave breaking before the waves reach the breakwater. For conditions with shallow water in front of the caisson breakwater, Goda (2009) proposed an expression, using $c = 1$ in Eq. (1), where the coefficients a and b depend on the relative water depth at the toe of the structure (H_{m0}/h) to incorporate the effect of shallow water in front of the caisson breakwater.

2.4. Recurved parapet

A recurved parapet (or bullnose or recurved wave return wall) can reduce wave overtopping. A recurved parapet consists of an overhang (with a length B_r) where the underside has the shape of a sector of a circle (with a radius R). After wave uprush along the vertical face of the structure, the water deflects seaward due to the overhang. The angle at the end of the circular part of the overhang is referred to as the exit angle α_E (where $\cos\alpha_E = (R–B_r)/R$). Fig. 2 shows a shape of a recurved parapet with the definition of the main parameters, here with an exit angle of 90°. The shape of the recurved parapet affects the influence on wave overtopping. Relatively low overtopping discharges go together with relatively thin layers of water reaching the parapet, resulting in an important effect on the amount of wave overtopping. For relatively high overtopping discharges the size of the parapet may be relatively small compared to the layers of water reaching the parapet, which can lead to a relatively small reduction in wave overtopping by the parapet.

To account for the effects of a recurved parapet on wave overtopping two types of methods have been proposed. The first method (hereafter "Method 1") is taking the influence of a recurved parapet into account by using a reduction factor in the general expression of wave overtopping as expressed in Eq. (1), which means that the ratio $\gamma_p = \ln(Q_{without\ parapet})/\ln(Q_{with\ parapet})$ is used. This can be seen as a correction of the value for b in Eq. (1) to account for the presence of the recurved parapet. This method is for instance applied by Franco and Franco (1999) in their study on the influence of oblique waves on wave overtopping at caisson breakwaters. The second method (hereafter "Method 2") is based on predicting the ratio between the amount of overtopping with and without a recurved parapet: (Kortenhaus et al., 2003; Pearson et al., 2004): $k = Q_{with\ parapet}/Q_{without\ parapet}$. This can be seen as a correction of the value for a in Eq. (1) to account for the presence of the recurved parapet.

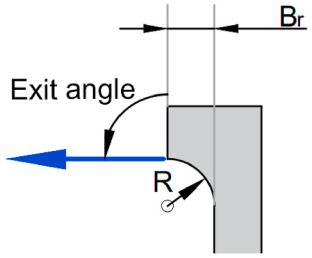

Fig. 2. Shape of recurved parapet.

Fig. 3 illustrates the two methods with the non-dimensional overtopping discharge on the logarithmic vertical axis and the relative freeboard on the linear horizontal axis. The black line in Fig. 3 reflects Eq. (1) using $a = 0.1$, $b = 3$ and $c = 1$ (*i.e.* values close to those applied by Franco and Franco, 1999). The green line illustrates Eq. (1). using $\gamma_p = 0.85$ to account for the presence of a specific recurved parapet ("Method 1"). In contrast to Method 2, for Method 1 no clear empirical expression reflecting the influence of the shape of the parapet is available. The black-dashed line in Fig. 3 illustrates Eq. (1). using a correction $k = 0.2$ on the coefficient a ("Method 2"). A constant factor for k as applied for the black-dashed line does not adequately reflect the influence of a recurved parapet since the parapet has a relatively large influence on lower overtopping discharges while for high overtopping discharges the influence is relatively low. Thus, a constant factor for k is not appropriate. Kortenhaus et al. (2003) and Pearson et al. (2004) proposed three regimes for the influence factor k using Method 2, where no effect of the parapet ($k = 1$) is present for low freeboards (low values of R_c/H_s), a factor that is close to a constant value ($k = 0.2$) for high freeboards, and a transition regime in between where the factor k again depends on the freeboard. The red line in Fig. 3 illustrates the method proposed by Pearson et al. (2004) for a configuration of the recurved parapet that has been used in the present study. The magnitude of the layers of water reaching the recurved parapet are not only dependent on the freeboard (R_c/H_s) but also on for instance the angle of wave attack. Therefore, the method proposed by Kortenhaus et al. (2003) and Pearson et al. (2004) is less suitable to be applied in combination with a reduction factor for oblique wave attack $\gamma = \gamma_\beta$ in Eq. (1); the transition from one regime of k to another is likely to depend not only on the freeboard and shape of the

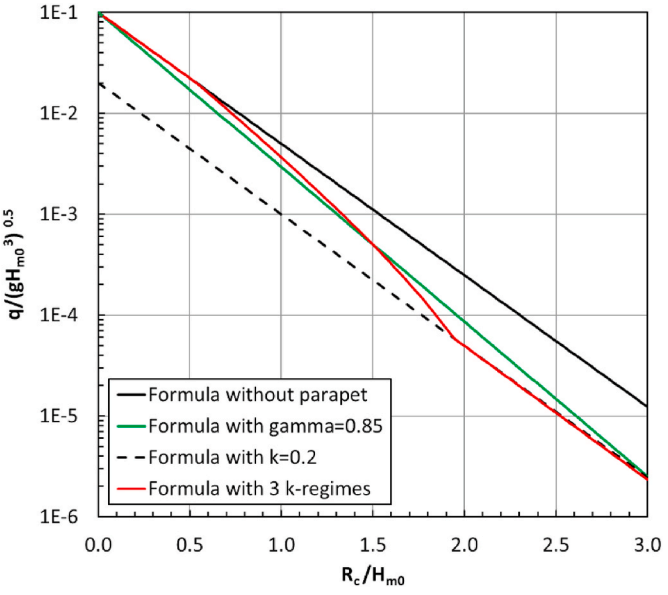

Fig. 3. Illustration of methods to account for the effects of a parapet on the amount of wave overtopping.

parapet, but also on the angle of wave attack. For this reason, Method 2 has not been applied in the present study.

The influence of the shape of the parapet was studied in detail by for instance Kortenhaus et al. (2003) and Pearson et al. (2004). Martinelli et al. (2018) more specifically demonstrated the importance of the exit angle of recurved parapets on wave overtopping. For an exit angle of 90° the effectiveness of the recurved parapet is optimal with respect to the reduction in wave overtopping (yet with a potential increase of wave forces). The present research is focussed on a comparison between a configuration without a recurved parapet and a recurved parapet with an exit angle of 90°.

2.5. Oblique waves

Here, an overview is given of available expressions to take the influence of oblique waves on wave overtopping into account for so-called non-impulsive wave loading on caisson breakwaters. For impulsive wave conditions Napp et al. (2004) provides guidance. The influence of oblique waves on wave overtopping discharges at caisson breakwaters under non-impulsive wave loading has been studied by Franco and Franco (1999); expressions for long-crested waves and for short-crested waves were proposed (in combination with Eq. (1) using $c = 1$). For long-crested waves:

$$\gamma_\beta = \cos\beta \text{ for } 0° \leq \beta \leq 37° \text{ and } \gamma_\beta = 0.79 \text{ for } \beta \geq 37° \quad (2)$$

For short-crested waves (rewritten to exclude the influence of directional spreading on the discharge for perpendicular waves):

$$\gamma_\beta = 1 \text{ for } 0° \leq \beta \leq 20° \text{ and } \gamma_\beta = \cos(\beta - 20°) \text{ for } \beta \geq 20° \quad (3)$$

Goda (2009) proposed the following expression, also in combination with Eq. (1) using $c = 1$:

$$\gamma_\beta = 1 - 0.0096|\beta| + 0.000054\,\beta^2 \quad (4)$$

EurOtop manual (2007), hereafter EM2007, proposed the following expression using Eq. (1) with $c = 1$:

$$\gamma_\beta = 1 - 0.0062|\beta| \text{ for } 0° \leq \beta \leq 45° \text{ and } \gamma_\beta = 0.72 \text{ for } \beta \geq 45° \quad (5)$$

EurOtop manual (2018), hereafter EM2018, proposed the following expression, rewritten here to match with Eq. (1). In EM2018 Eq. (1) is used with $c = 1.3$. For long-crested waves:

$$\gamma_\beta = (1 - 0.0062|\beta|)^{1.3} \text{ for } 0° \leq \beta \leq 45° \text{ and } \gamma_\beta = 0.72^{1.3} = 0.652 \text{ for } \beta \geq 45° \quad (6)$$

For short-crested waves:

$$\gamma_\beta = (1 - 0.0033|\beta|)^{1.3} \text{ for } 0° \leq \beta \leq 80° \text{ and } \gamma_\beta = 0.736^{1.3} = 0.671 \text{ for } \beta \geq 80° \quad (7)$$

Fig. 4 shows Eqs. (2)–(7). Fig. 4 shows that all expressions except those by Franco and Franco (1999) show an important reduction already for small wave angles. A relatively strong influence for small wave angles was not observed for sloping coastal structures, see for instance Van Gent and Van der Werf (2018) for rubble mound structures with a crest wall and Van Gent (2020) for dikes. Due to lack of data for large wave angles either the expressions are not extrapolated to large angles or a constant value is proposed for large wave angles, leading to sharp transitions from one part of the expression to a horizontal line. Only the expression by Franco and Franco (1999) for short-crested waves and the expression by Goda (2009) show more natural shapes without sharp transitions.

Note that all expressions shown in Fig. 4 are for the reduction factor γ in the exponential part of expression of Eq. (1) such that the actual influence of the wave angle on the overtopping discharge is much larger than the linear scale shown in Fig. 4 could suggest.

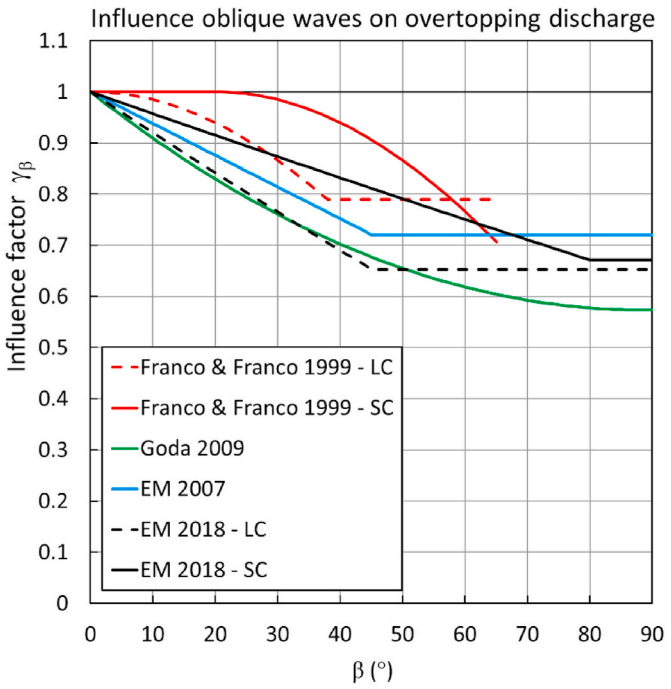

Fig. 4. Influence factors for oblique waves and non-impulsive conditions (LC: for long-crested waves; SC: for short-crest waves).

2.6. Crossing seas

Crossing seas are wave conditions with simultaneously another wave condition from another wave direction. For more information on crossing seas, see for instance Petrova et al. (2013) and Petrova and Guedes Soares (2014). All available expressions for wave overtopping at caisson breakwaters are for single sea states of wind generated waves. For wave loading conditions that consist of two simultaneous sea states of incident waves, each from a different wave direction, Van der Werf and van Gent (2018) proposed an influence factor for crossing seas ($\gamma_\#$), while if the wave loading consists of a wind waves plus swell, a method is proposed to account for the swell conditions by reducing the effective freeboard. Van der Werf and van Gent (2018) tested a sloping structure (with wave angles $\beta = \pm 45°$). See also Vieira Leite et al. (2019) for tests with crossing seas and a sloping structure. For caisson breakwaters no prediction method for multiple sea states is available. Therefore, in the present tests also conditions with sea conditions from one direction and simultaneous swell conditions from another direction are included.

3. Physical model tests

3.1. Test set-up

The physical model tests on vertical caisson breakwaters were performed in the Delta Basin at Deltares. The multi-directional wave generator consists of 100 paddles and is equipped with active reflection compensation. This means that the motion of the wave paddles compensates for the waves reflected by the caisson breakwater, preventing them to re-reflect at the wave paddles and propagate towards the model, causing an unrealistic amount of wave energy and an unrealistic wave field in the wave basin. The active wave absorption system accounts for 3D effects and short-waves effects. This means that the direction of the reflected waves propagating towards the wave board is accounted for and that the reflected waves propagating towards the wave board are absorbed accounting for short-waves effects and not only for long-waves effects. For coastal structures such as caisson breakwaters that cause a significant amount of wave reflection, this system is essential to prevent

that the measurements are disturbed by unphysical re-reflected waves. The applied wave generation and wave absorption method is based on Wenneker et al. (2010).

Fig. 5 shows the layout of the model in the wave basin with the wave generator at the bottom of the figure. The foreshore was horizontal. The length of the vertical caisson breakwater was 22.1 m. The angle between the structure and the wave generator was 17°. The side wall at the right-hand side of Fig. 5 was used to obtain the required wave conditions over the entire length of the structure via reflection against this side wall. At four positions wave overtopping discharges were measured, three along the trunk of the breakwater (*q1* to *q3* in Fig. 5) and one close to the corner of the breakwater (*q4* in Fig. 5). The mean overtopping discharge was measured by collecting the overtopping water via an overtopping chute (each over a width of 0.80 m) into overtopping boxes that were constructed inside the caisson (see also Fig. 6). A pumping system was installed in each box, but these were not used during a test since the overtopping boxes were large enough to collect all overtopping water during a single test.

Fig. 6 shows the cross-section of the tested structure without a recurved parapet. The green dashed lines indicate the actual profile of the modelled caisson breakwater. The overtopping box was constructed inside the caisson breakwater. For those test series where a recurved parapet was used the configuration of the parapet as shown in Fig. 2 with $R = 8$ mm, $B_r = 8$ mm and an exit angle of 90° was used. The caisson was fixed on an impermeable concrete bed. The upper-left panel of Fig. 7 shows the model in the dry wave basin; the panel below shows an overview of the model in the wave basin with the wave generator on the right-hand side (with long-crested waves). The other panels of Fig. 7 show details of the model and overtopping events during a test with oblique waves (*i.e.* long-crested waves with an incident wave angle of 45° and the largest wave steepness).

3.2. Test programme

Waves were measured on the horizontal foreshore by using a directional wave gauge (GRSM) such that incident and reflected waves can be separated (see also Fig. 5). Calibration tests without the structure in position were performed and the analysis was based on the measured incident waves at the position of wave overtopping box q2. The spectral incident significant wave height H_{m0} and the spectral wave period $T_{m-1,0}$ were obtained from the measured wave energy spectra. In all tests a JONSWAP wave spectrum (with a peak enhancement factor of 3.3) has been applied for the sea states. All tests consisted of 1 000 waves. Each configuration was tested with a constant target wave steepness of either $s_{m-1,0} = 0.02$ or $s_{m-1,0} = 0.04$. For each wave steepness three different wave heights were tested. Tests were performed with long-crested waves (unidirectional waves) and with short-crested waves (multi-directional waves). In all tests with short-crested waves the amount of directional spreading was constant (normal distribution with $\sigma = 25°$). The wave directions that were tested were $\beta = 0°$, 15°, 30°, 45°, 60° and 75°, where 0° corresponds to perpendicular wave attack. This leads to 36 tests per series of tests.

In addition, also tests with a combination of two simultaneous wave conditions were performed, one with a short-crested sea state and one with a long-crested swell condition. In these bimodal conditions the sea conditions were identical to those described above (with $s_{m-1,0} = 0.02$ or $s_{m-1,0} = 0.04$) while the swell conditions were generated using a Pierson-Moskowitz spectrum with a target wave height of $H_{m0\text{-swell}} = 0.04$ m and a constant wave steepness of either $s_{m-1,0} = 0.0012$ or $s_{m-1,0} = 0.0061$. In these bimodal tests the selection of combined wave directions was: $\beta_{sea} = 0°$ with $\beta_{swell} = 0°$, 30° and 60°, $\beta_{sea} = 30°$ with $\beta_{swell} = 0°$, and $\beta_{sea} = 60°$ with $\beta_{swell} = 0°$. The combination of $\beta_{sea} = 0°$ with $\beta_{swell} = 60°$ was tested for both values of the wave steepness; the other combinations were tested with $s_{m-1,0} = 0.0061$ only. Thus, in total 36 conditions with bimodal conditions were tested.

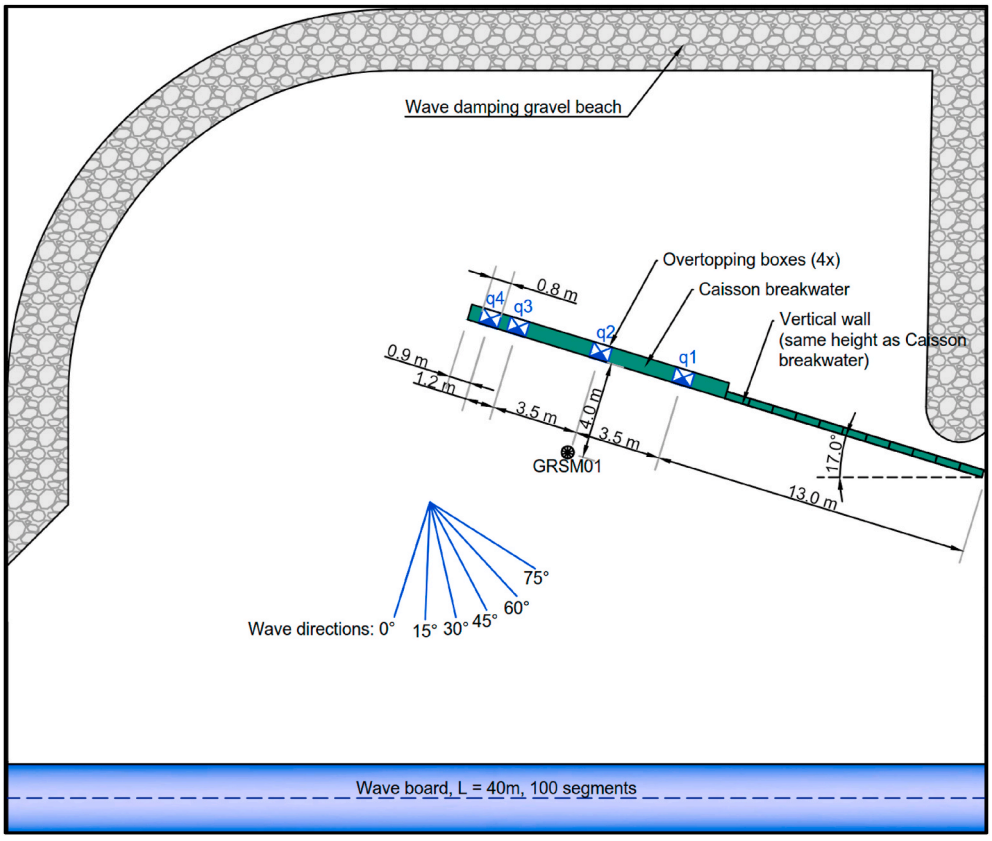

Fig. 5. Physical model set-up in wave basin.

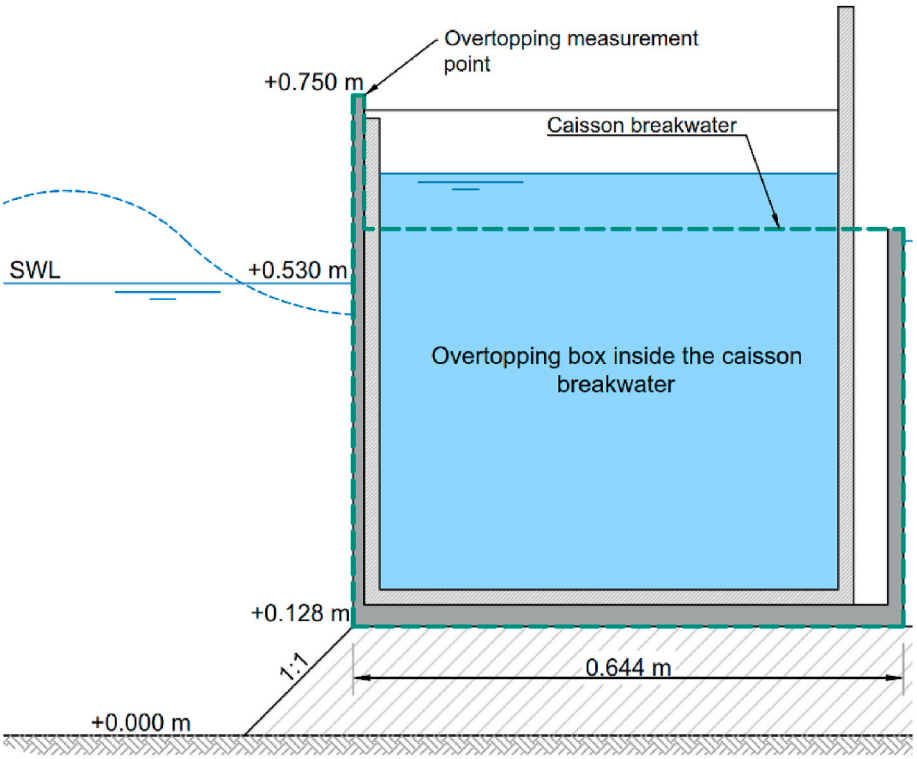

Fig. 6. Tested cross-section.

Table 1 shows the six test series, each with 36 test conditions. Two series have been performed with short-crested waves without a parapet, using two different water levels leading to two different freeboards. Two series have been performed with a recurved parapet, again using two different water levels leading to two different freeboards. One series with long-crested waves has been performed and one series with crossing seas. This results in a total of 216 tests of which three tests did not result in any wave overtopping. Table 2 shows the ranges of the most important parameters of the test programme.

3.3. Discussion of test set-up

Mase et al. (2002) addressed the presence of stem waves for (reflecting) vertical structures for conditions where the angle between the structure and the direction of wave propagation is small. Stem waves can potentially develop along the structure due to the interaction between incident and reflected waves. The height of the stem wave increases as the wave travels along the structure. For irregular waves a maximum increase in amplitude is reached after a number of wave lengths. For monochromatic incident waves the stem wave can relatively easily develop for small angles between the reflecting structure and the direction of wave propagation; for irregular waves the magnitude is smaller but can still reach a height twice the incident wave height. However, it is assumed that for short-crested waves (the vast majority of tests in the present test programme) the resonance between incident and reflected waves is much less than for long-crested (unidirectional) waves. Nevertheless, if stem waves occur these should be taken into account since they would also occur in reality. The influence of stem waves on the amount of overtopping, generally the result of the higher (non-linear) waves in the wave energy spectrum, is unknown. In the present test programme stem waves could potentially occur for the conditions where the angle between the structure and direction of propagation is 15° (in the test programme this is denoted by $\beta = 75°$).

4. Analysis of test results

4.1. Comparison between trunk sections and corner section

Three overtopping boxes were positioned in the trunk of the breakwater and one close to the tip of the breakwater (hereafter: corner), see also Figs. 5–7. Fig. 8 shows the comparison between the measured discharges at the trunk (*i.e.* the mean of the discharges at the three trunk sections *q1*, *q2* and *q3*) and at the corner (*q4*) for the data of the test series with short-crested waves, with and without a recurved parapet (*i.e.* Series A to D). If the discharges at the corner would be equal to those at the trunk, the data would have been on the full red lines in Fig. 8, with linear axes in the left panel to focus on the higher discharges, and logarithmic axes in the right panel. However, the data are closer to the red dashed lines since the overtopping discharges at the corner are on average somewhat higher than at the trunk. The physical process causing the observed somewhat higher overtopping discharge at the corner compared to the trunk is yet unknown. However, Ito and Tanimoto (1971) reported an expression and diagrams (see also Goda, 1985, Figs. 3.40, 3.44 and 3.45) that indicates that surface elevations increase near the corner. The higher discharge can be accounted for by using $\gamma = \gamma_{corner} = \ln Q_{trunk}/\ln Q_{corner} = 1.05$ in Eq. (1) (dashed lines in Fig. 8 indicate this value). For perpendicular wave attack the increase at the corner sections appears to be somewhat smaller ($\gamma_{corner} = 1.03$). Negligible systematic differences occurred between the three trunk sections; the average differences between the discharges measured in the three overtopping boxes in the trunk are: $\ln Q_{q1}/\ln Q_{q2} = 1.001$ and $\ln Q_{q2}/\ln Q_{q3} = 1.002$ for discharges larger than $Q = 10^{-6}$. In the further analysis, average of the four overtopping boxes has been used after accounting for the corner effect using $\gamma_{corner} = 1.05$ (also for perpendicular wave attack) for overtopping box q4 to obtain representative values for the trunk.

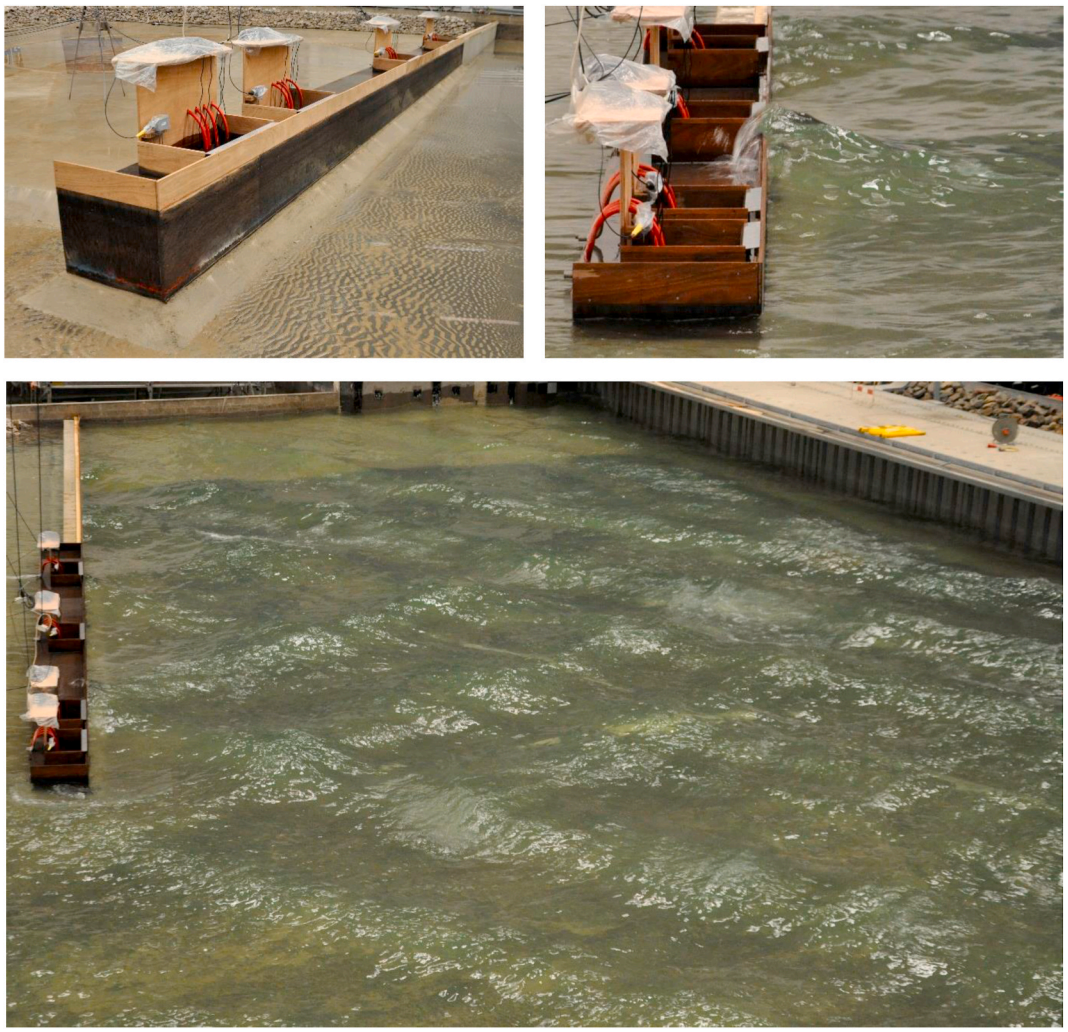

Fig. 7. View of the model in the dry wave basin in the upper-left panel, an overtopping event in the upper-right panel, overviews of the model in the wave basin in the next two panels with the wave pattern of incident and reflected waves (clapotis gaufré), and images of overtopping events in the lowest two panels.

4.2. Short-crested waves and structure without recurved parapet

Fig. 9 shows the data for the series with short-crested waves without a recurved parapet (Series A and B) with the non-dimensional discharge at the logarithmic vertical axes and the non-dimensional freeboard at the horizontal axes. The lines and curves in Fig. 9 will be explained later in this section.

The graphs in Fig. 9 show a clear dependency of the overtopping discharges on the angle of wave attack. The differences between discharges for perpendicular wave attack with $\beta = 0°$ (red) and the most oblique waves with $\beta = 75°$ (black) can reach an order of magnitude. For the same overtopping discharge, the required crest height can be about half a significant wave height lower for the most oblique waves compared to the required crest height for perpendicular waves.

The left panels in Fig. 9 show the data for the lower wave steepness ($s_{m\text{-}1,0} = 0.02$) while the right panels show the higher wave steepness ($s_{m\text{-}1,0} = 0.04$). Although for several conditions there are clear differences between tests with a lower and with a higher steepness, the influence of the wave steepness is for most tested conditions not significant, at least clearly less than the differences observed as a result of the variations in freeboard and angle of wave attack. As indicated by Eq. (1), previous research also did not show a clear systematic dependency on the wave steepness for non-impulsive wave loading (the wave steepness or wave period is not present in Eq. (1)). The further analysis described here does not focus on a better description of the influence of the wave steepness; other parameters are more important.

Obviously, also the dependency on the freeboard is clear for each of the angles of wave attack. The dependency on the freeboard is expressed by Eq. (1). First the coefficients have been calibrated based on the tests for perpendicular wave attack. This has been done both for a value $c = 1$ and for a value $c = 1.3$. Use is made of the following error-measure, referred to as RMSE:

$$\mathrm{RMSE} = \sqrt{\frac{\sum_{i=1}^{n_{tests}} \left(\log(Q_{measured}) - \log(Q_{calculated})\right)^2}{n_{tests}}} \tag{8}$$

where n_{tests} is the number of tests on which the RMSE is based, Q are the non-dimensional values of the measured and calculated overtopping discharges [$Q = q/(gH_{m0}^3)^{0.5}$]. The RMSE is only based on measured overtopping values larger than $Q = 10^{-6}$ since smaller values are often less relevant and scale effects may be present. Table 3 shows the RMSE values for perpendicular wave loading in the last-but-one column. The values for a are equal to those proposed by Franco et al. (1994) for $c = 1.0$ and by EM2018 for $c = 1.3$. The calibrated values for b are somewhat smaller than proposed before (Franco et al., 1994, proposed $b = 4.3$ using $c = 1.0$ while EM2018 proposed $b = 3.04$ using $c = 1.3$).

To account for the effects of oblique waves use is made of the following expression, see also Van Gent (2014, 2020) and Van Gent and van der Werf (2019):

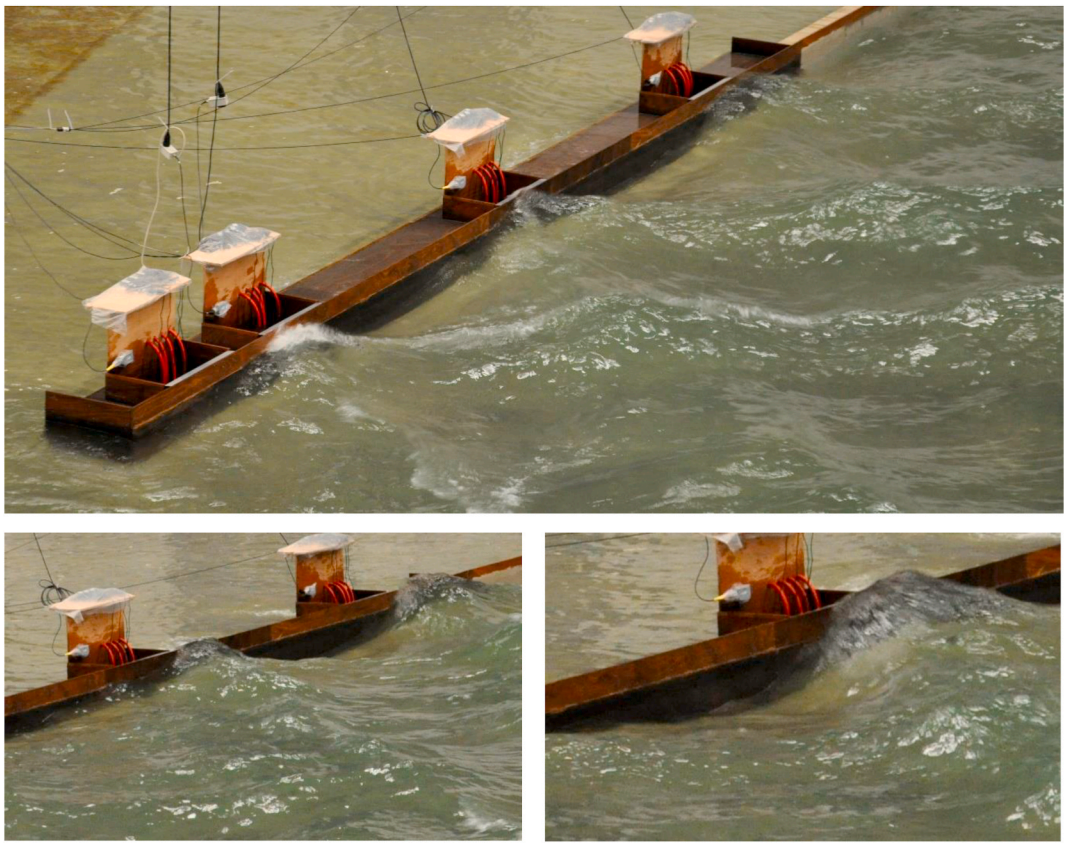

Fig. 7. (*continued*).

Table 1
Test series.

Series	Main characteristics	R_c (m)
A	Short-crested waves; no recurved parapet	0.200
B	Short-crested waves; no recurved parapet	0.220
C	Short-crested waves; with recurved parapet	0.167
D	Short-crested waves; with recurved parapet	0.187
E	Long-crested waves; no recurved parapet	0.220
F	Crossing seas (Sea: short crested, Swell: long-crested); no recurved parapet	0.220

Table 2
Parameter ranges of the test programme (model scale).

Parameter	Symbol	Values/Range
Water depth (m)	h	0.530–0.600
Freeboard (m)	R_c	0.167–0.022
Non-dimensional freeboard (−)	R_c/H_{m0}	1.2–2.9
Incident wave height at toe: sea states (m)	H_{m0}	0.076–0.155
Incident wave height at toe: swell (m)	$H_{m0\text{-}swell}$	0.036–0.042
Wave steepness: sea states: $s_{m\text{-}1,0} = 2\pi H_{m0}/gT^2_{m\text{-}1,0}$ (−)	$s_{m\text{-}1,0}$	0.015–0.041
Wave steepness: swell: $s_{m\text{-}1,0} = 2\pi H_{m0}/gT^2_{m\text{-}1,0}$ (−)	$s_{m\text{-}1,0\text{-}swell}$	0.0013–0.0070
Wave angles at structure of sea states (°)	β	0, 15, 30, 45, 60, 75
Wave angles at structure of swell (°)	β_{swell}	0, 30, 60
Number of waves (−)	N	1 000
Overtopping discharge (l/s/m)	q	0–0.20
Non-dimensional overtopping discharge (−)	$Q = q/(gH^3_{m0})^{0.5}$	0–0.0012

$$\gamma_\beta = (1 - c_\beta)\cos^2\beta + c_\beta \tag{9}$$

The optimal value for the coefficient c_β depends on the expression in which it is used, including the value of the coefficient c in Eq. (1). For short-crested waves without a recurved parapet the optimal values are $c_\beta = 0.75$ if $c = 1$ is used in Eq. (1) ($\gamma = \gamma_\beta$) and $c_\beta = 0.70$ if $c = 1.3$ is used. The calibration of Eqs. (1) and (9) (based on Series A and B) leads to the RMSE in the last column of Table 3. Table 3 shows that the differences between the RMSE using $c = 1$ or $c = 1.3$ hardly show any difference.

The values of Table 3 are used in Figs. 9 and 10. The upper graphs in Fig. 9 show lines using $c = 1$ in Eq. (1). while the lower graphs show curves using $c = 1.3$ in Eq. (1). Fig. 9 indicates that the data do not clearly support the use of one value for c in favour for another; both values can be used to estimate the dependency on the freeboard. Fig. 10 shows the measured discharges versus the calculated values using Eqs. (1) and (9) with $a = 0.2$, $b = 3.9$, $c = 1.0$ and $c_\beta = 0.75$ in the upper panels and $a = 0.047$, $b = 2.57$, $c = 1.3$ and $c_\beta = 0.70$ in the lower panels. The left panels show the data using linear axes (to focus on the higher discharges) and the right panels show the same data using logarithmic axes. Fig. 10 shows a reasonable match between the measured and calculated discharges. For the higher overtopping discharges (see left panels) there seems to be no influence of the wave steepness, while the lower discharges for the lower wave steepness (see right panels) are on average overpredicted; the lower steepness leads to somewhat lower discharges than the corresponding conditions with a higher steepness. Nevertheless, the match for discharges larger than $Q = 10^{-5}$ is quite good (note that $Q = 10^{-5}$ corresponds to a discharge of $q = 1$ l/s/m for waves with $H_{m0} = 10$ m, or to $q = 0.032$ l/s/m for waves with $H_{m0} = 1$ m; smaller discharges are often less relevant).

4.3. Recurved parapet

In the test programme one shape of the recurved parapet has been used (with an exit angle of 90°, see Fig. 2). Therefore, the influence of the presence of a recurved parapet can be studied but not the influence of the shape of the parapet itself. Based on the tests with and without a recurved parapet the influence factor of the recurved parapet $\gamma = \gamma_p = \ln$

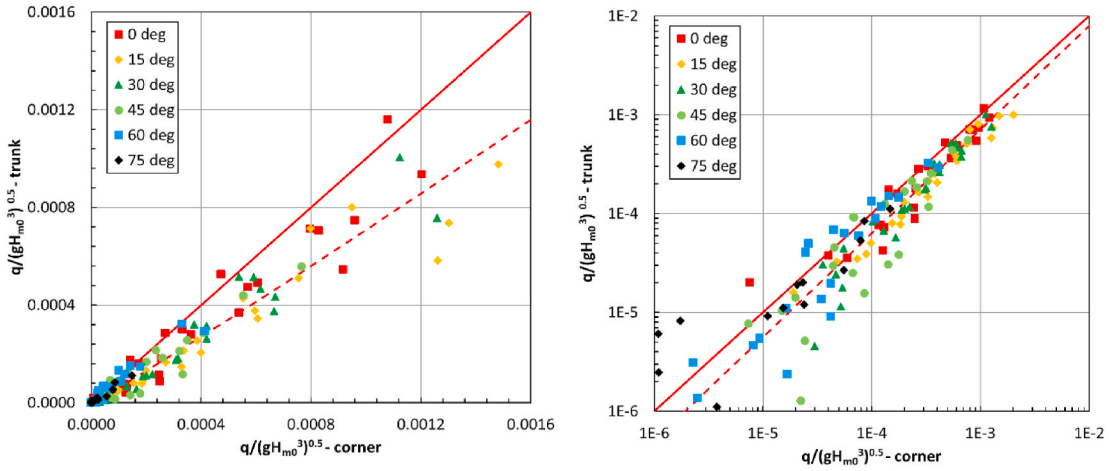

Fig. 8. Measured non-dimensional overtopping discharges at the trunk sections (*q1*, *q2* and *q3*) versus the discharge measured at the corner section (*q4*); left panel with linear axes, right panel with logarithmic axes.

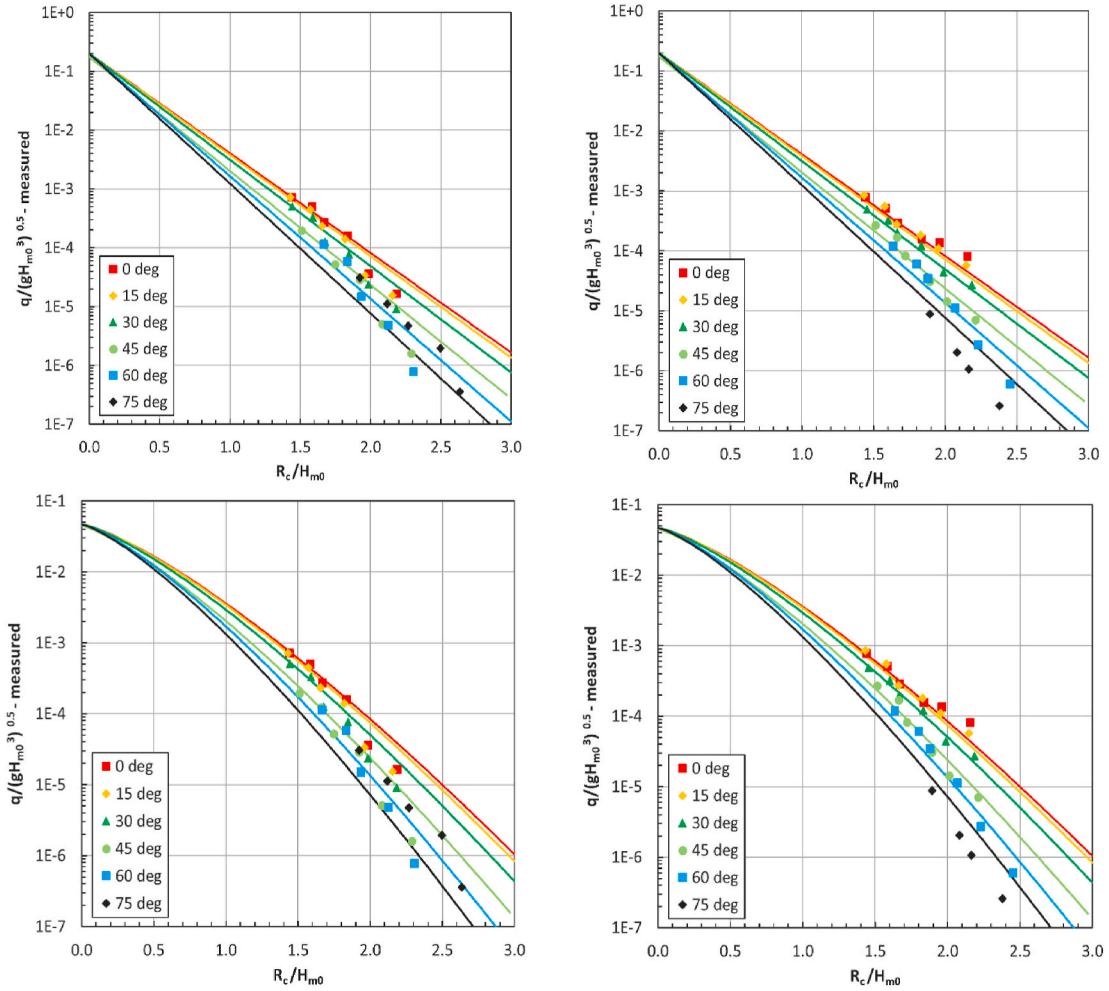

Fig. 9. Measured overtopping discharges for short-crested waves versus freeboard (non-dimensional): Left panels for lower wave steepness, right panels for higher wave steepness; upper panels for $c = 1$ and lower panels for $c = 1.3$ in Eq. (1).

$Q_{without\ parapet}$/ln $Q_{with\ parapet}$ can be determined based on the conditions with perpendicular short-crested waves (using Series A to D, see Table 4).

For oblique waves it appeared that the influence of the recurved parapet reduces for larger wave angles. This seems reasonable since for waves propagating along the structure ($\beta = 90°$) the parapet is expected not to affect the flow over the structure as it does for smaller wave angles. The following expression to account for the combined effects of oblique waves and of a recurved parapet appears to lead to a good match with the test results, leading to a maximum effect of the recurved

Table 3
Short-crested waves without parapet: RMSE for perpendicular wave attack and RMSE for all wave directions.

Coefficient c in Eq. (1)	a	b	c_β	RMSE-perp.	RMSE-all
$c = 1.0$	0.2	3.9	0.75	0.182	0.240
$c = 1.3$	0.047	2.57	0.70	0.182	0.245

parapet for perpendicular waves ($\beta = 0°$) and no effect of the recurved parapet for waves propagating along the structure ($\beta = 90°$); note that $\gamma = \gamma_\beta \gamma_p$ in Eq. (1):

$$\gamma_\beta = \left(1 - \frac{c_\beta}{\gamma_p}\right)\cos^2\beta + \frac{c_\beta}{\gamma_p} \tag{10}$$

Fig. 11 shows Eq. (10) for the structures with and without the recurved parapet. A less effective recurved parapet, for instance a similar recurved parapet but with a smaller exit angle than the tested exit angle of 90°, would result in a higher value of γ_p (*i.e.* $0.85 < \gamma_p < 1$) and for such a recurved parapet the curve for γ_β would be between the two curves shown in Fig. 11. A recurved parapet that would be more effective than the one tested ($\gamma_p < 0.85$) would result in a curve for γ_β above the upper one in Fig. 11. For all shapes of the recurved parapet, the combined influence of oblique waves and a recurved parapet results in a value of $\gamma = \gamma_\beta \gamma_p = c_\beta$ for waves propagating along the structure ($\beta =$ 90°). Note that long-crested waves can reach the structure under this mean wave angle ($\beta = 90°$) but short-crested waves cannot; a mean wave angle of the incident waves of $\beta = 90°$ is impossible for short-crested (multi-directional) waves since a part of the (offshore) directions would not reach the structure leading to a smaller mean angle of the incident waves.

Fig. 12 shows the measured versus the calculated overtopping discharges, using Eqs. (1) and (10), (see also Table 4). The left panel, with linear axes, shows that the match between both is reasonably good although the larger discharges are somewhat underestimated for some of the wave angles (mainly for $\beta = 15°$ and 30°). The right panel of Fig. 12, with logarithmic axes, shows that for the smaller discharges (mainly for $\beta = 75°$) the discharges are somewhat overestimated. Nevertheless, the match for discharges larger than $Q = 10^{-5}$ is quite good.

Table 4
Short-crested waves with parapet: RMSE for perpendicular wave attack and RMSE for all wave directions.

Coefficient c in Eq. (10)	a	b	c_β	γ_p	RMSE-perp.	RMSE-all
$c = 1.0$	0.2	3.9	0.75	0.89	0.112	0.192
$c = 1.3$	0.047	2.57	0.70	0.85	0.105	0.178

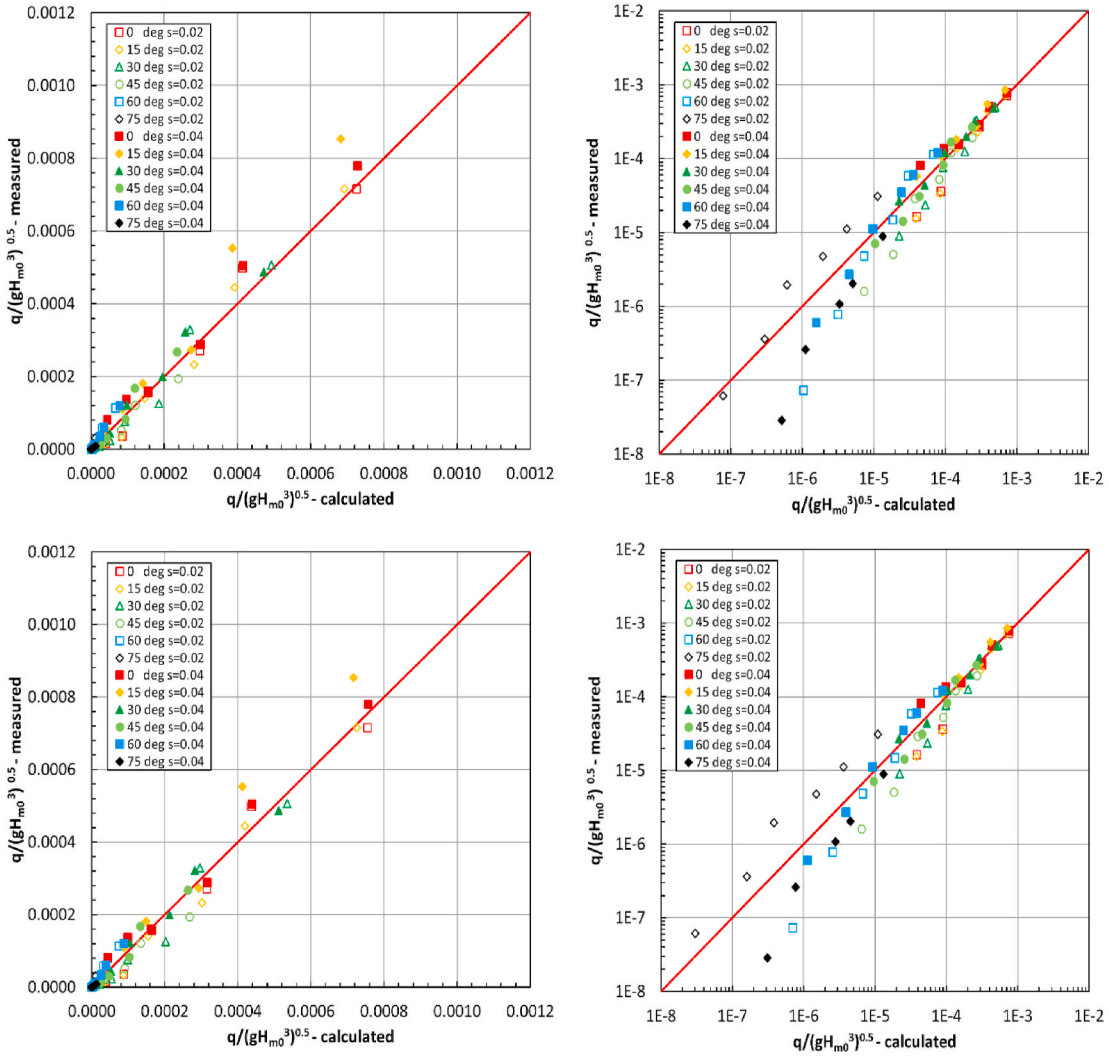

Fig. 10. Measured versus calculated overtopping discharges using $a = 0.2$, $b = 3.9$, $c = 1.0$ and $c_\beta = 0.75$ in Eqs. (1) and (9) in the upper panels and $a = 0.047$, $b = 2.57$, $c = 1.3$ and $c_\beta = 0.70$ in the lower panels; left panels with linear axes, right panels with logarithmic axes.

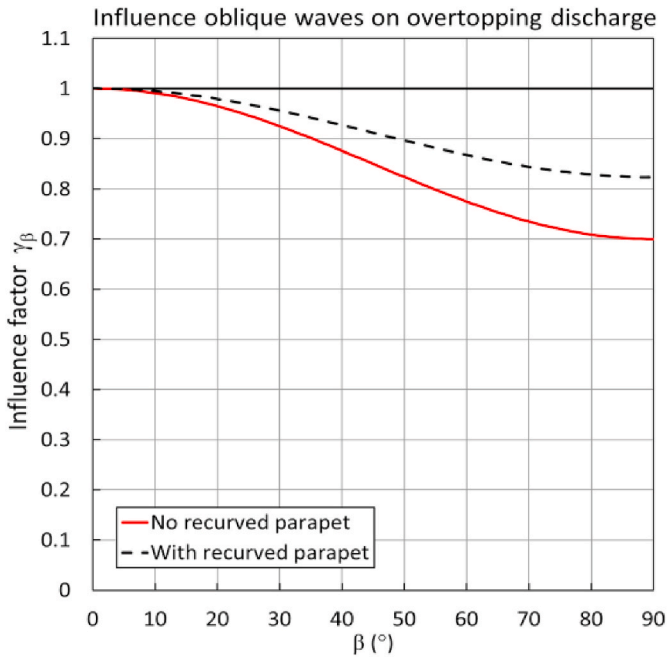

Fig. 11. Influence of short-crested oblique waves for structures with and without a recurved parapet ($c = 1.3$ in Eq. (1)).

4.4. Long-crested waves

To analyse potential differences between long-crested waves (uni-directional waves) and short-crested waves (multi-directional waves), Series E has been performed with long-crested waves.

For long-crested waves the value for the coefficient b in Eq. (1) appears to be slightly larger than for short-crested waves (Table 5). Note that the calibration of the coefficient is based on conditions with perpendicular waves (*i.e.* six tests) and that the values for b are also affected by a single test with a discharge that deviates from the trend through the other five tests with perpendicular waves. For oblique waves the discharges for the most oblique waves ($\beta = 75°$) are significantly lower than for the other wave directions. If stem waves (see also Section 3.3) would be the cause of these deviations from the trend, the effect of stem waves would be a reduction in overtopping discharge.

The optimal values for the coefficient c_β to account for the effects of oblique waves are somewhat higher than those for short-crested waves. This is different from other observations where the influence of oblique waves on the overtopping discharges either are the same for long-crested waves (*e.g.* Van Gent and van der Werf, 2019, for a crest wall on top of a rubble-mound breakwater) or smaller (*e.g.* Franco and Franco, 1999, for a caisson structure). The RMSE are clearly larger for long-crested waves than for short-crested waves. This larger scatter is also visible in Fig. 13, where the left panel (linear axes) focusses on the larger overtopping discharges. The right panel (logarithmic axes), shows that the scatter is large for the low overtopping discharges, especially for the most oblique waves ($\beta = 75°$).

4.5. Crossing seas

For some locations dominant sea states go together with swell. However, all available expressions for wave overtopping at caisson breakwaters are for single sea states of wind generated waves. For wave loading conditions that consist of two simultaneous conditions, each from a different wave direction, Van der Werf and van Gent (2018) proposed a method to account for the swell conditions by reducing the effective freeboard. However, that method was developed for sloping structures. Using the same method for vertical caisson breakwaters would lead to the following expression for bimodal wave conditions that consist of a sea and swell component:

$$\frac{q}{\sqrt{gH_{m0}^3}} = a \exp\left[-\frac{b}{\gamma_\beta \gamma_p}\left(\frac{R_c - c_{swell}H_{m0-swell}}{H_{m0}}\right)^c\right] \quad (11)$$

where H_{m0} is the spectral wave height of the incident waves of the wind waves (thus excluding the swell condition), $H_{m0\text{-}swell}$ is the spectral wave height of the incident waves of the swell, γ_β denotes the influence factor for the angle of wave attack based on the wave angle of the wind waves (thus independent of the direction of swell), γ_p denotes the influence of a recurved parapet ($\gamma_p = 1$ in case no recurved parapet is present), coefficients a, b and c are those obtained for single sea states (*i.e.* wind

Table 5
Long-crested waves: RMSE for perpendicular wave attack and RMSE for all wave directions.

Coefficient c in Eq. (1)	a	b	c_β	RMSE-perp.	RMSE all
$c = 1.0$	0.2	4.0	0.8	0.330	0.280
$c = 1.3$	0.047	2.7	0.8	0.315	0.278

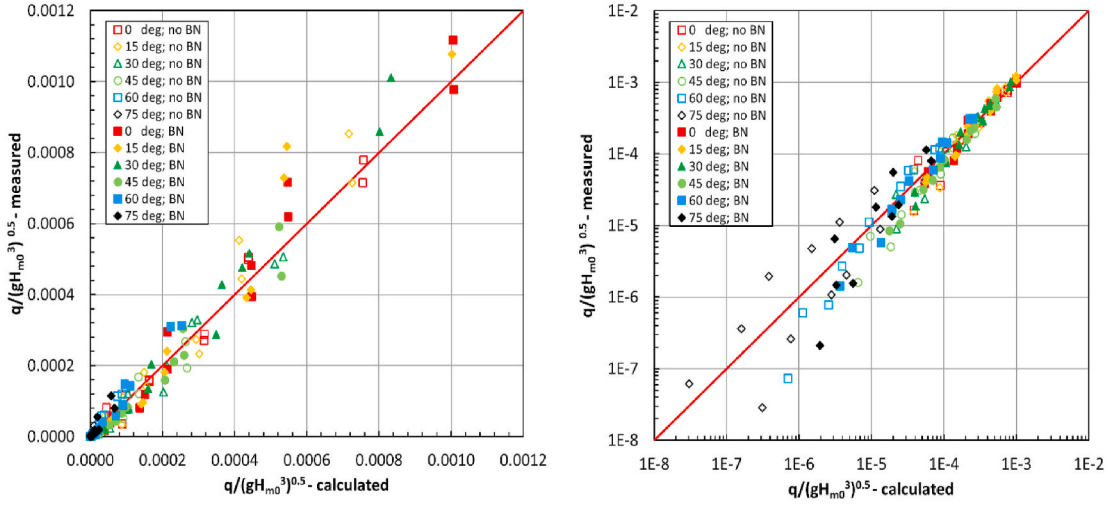

Fig. 12. Measured versus calculated overtopping discharges for structures with (denoted by "BN") and without recurved parapet or bullnose (denoted by "no BN") ($a = 0.047$, $b = 2.57$, $c = 1.3$, $c_\beta = 0.70$ and $\gamma_p = 0.85$ in Eqs. (1) and (10); left panel with linear axes, right panel with logarithmic axes.

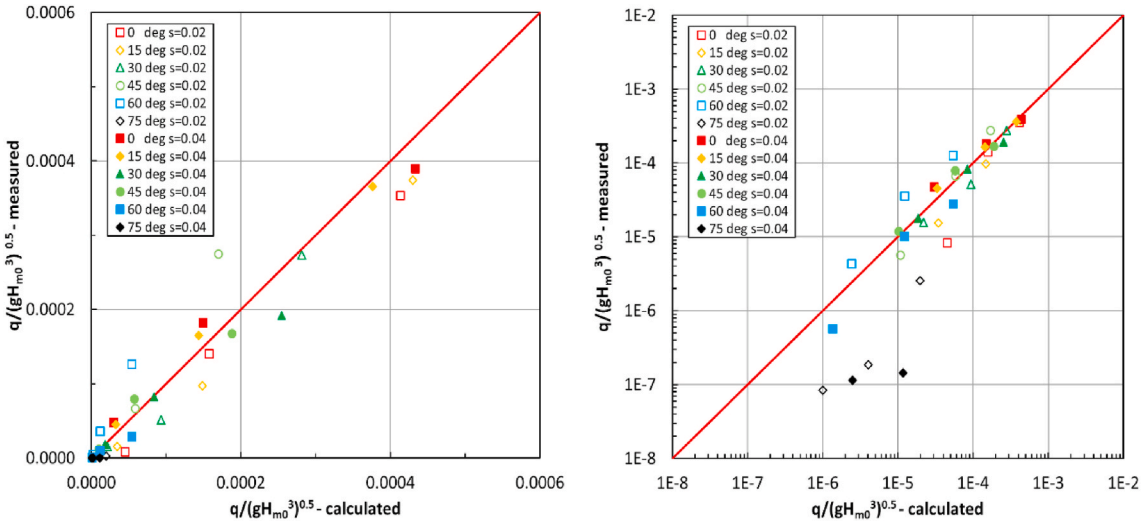

Fig. 13. Measured versus calculated overtopping discharges for long-crested waves ($a = 0.047$, $b = 2.7$, $c = 1.3$ and $c_\beta = 0.8$ in Eqs. (1) and (9); left panel with linear axes, right panel with logarithmic axes.

waves) and c_{swell} is the coefficient to account for the reduced effective freeboard due to the presence of swell (Van der Werf and van Gent, 2018, proposed $c_{swell} = 0.5$ based on tests with a sloping structure). The swell is included in Eq. (11) as an increase of the water level (or decrease of the effective freeboard) that is close to half of the height of the swell component, irrespective of the direction of the swell. This way, the effect of the swell is accounted for as an increase of the water level to a level that is close to the crest level of a representative wave of the swell for which H_{m0} is used; the wind waves propagate towards the structure as if the water level is (temporarily) higher due to the presence of swell. Based on the present tests the optimal value for c_{swell} appears to be $c_{swell} = 0.4$ (RMSE for $c_{swell} = 0$, 0.3 or 0.5 are higher, see also Table 6 to illustrate this).

The conditions including swell can be compared to conditions without swell since the values of R_c- 0.4 $H_{m0\text{-}swell}$ are 0.204 m for all conditions with swell (Serie F: $R_c = 0.22$ m; $H_{m0\text{-}swell} = 0.04$ m) while the corresponding tests without swell have been tested as well (Series A: $R_c = 0.20$ m; $H_{m0\text{-}swell} = 0$ m), thus the effective freeboard is similar (0.204 m versus 0.200 m). The left panel of Fig. 14 shows the comparison of the tests with and without swell. The rather good match between both indicates that the swell can indeed be accounted for using the reduced freeboard R_c - 0.4 $H_{m0\text{-}swell}$. Using Eq. (11) leads to the comparison between measured and calculated discharges shown in the right panel of Fig. 14 and the RMSE shown in Table 6. Fig. 14 and the RMSE show that sea states in combination with swell can be accounted for accurately using Eq. (11) with Eq. (9) (*i.e.* Eq. (10) with $\gamma_p = 1$).

4.6. Discussion of results

Fig. 15 shows all overtopping discharges measured for long-crested waves, short-crested waves, combinations of sea and swell, and for caisson structures with and without recurved parapet (with recurved parapet is denoted by "BN"). The discharges are for trunk sections. For corner sections the discharges are larger than for trunk sections, and this increase can be accounted for by incorporating an influence factor γ_{corner} in Eq. (1) or Eq. (11) (*i.e.* for a corner section the value b should be divided by $\gamma_{corner} = 1.05$). For example, for waves with $H_{m0} = 5$ m that lead to $q = 10$ l/s/m at the trunk, the discharge would become $q = 13.7$ l/s/m at the corner section. Whether higher overtopping discharges than at the trunk can be tolerable depends on the presence of facilities near the corner.

Fig. 15 shows that Eq. (11) with Eq. (10) to account for the influence of oblique waves describes most of the data accurately. The conditions with long-crested waves approaching under the most oblique wave angle ($\beta = 75°$) contribute the most to the scatter. As discussed, the potential reason is the presence of stem waves for these very oblique long-crested waves.

Eq. (10) describes the influence of oblique waves on wave overtopping at caisson breakwaters. Without recurved parapet this expression is equal to Eq. (9). To provide further insight into the spreading in the results using the proposed method, the value of γ_β that would lead to a perfect match between the measured and the calculated discharge is calculated for each test. This means that all potential inaccuracies of the applied overtopping formula (Eq. (11)), the applied method to account for a recurved parapet (*i.e.* one value of γ_p for all conditions), and the applied method to account for oblique waves (Eq. (10)), all affect the obtained values of γ_β (thus not only inaccuracies in the method to account for oblique waves affect these values). Fig. 16 shows the resulting values for γ_β for (a) Short-crested waves, including the conditions with simultaneous sea and swell, for the structures without recurved parapet, (b) Short-crested waves, for the structures with a recurved parapet, and (c) Long-crested waves. The corresponding curves of Eq. (11) are shown here using $c = 1.3$ in Eq. (10). On average the curves provide a trend through the data-points except for some of the tests with the most oblique wave angle (long-crested waves with $\beta = 75°$). Note that some of the shown data points are for discharges lower than $Q = 10^{-6}$; those they have not been used in the calibration of the coefficients, since very small discharges may not be of practical relevance or may be affected by scale-effects.

Eq. (11) is an extension of Eq. (1) to account for the simultaneous presence of sea and swell. Eq. (1) has been used for single sea states (*i.e.* wind waves) by various authors using different values for a, b and c. Table 7 shows these values and the corresponding RMSE based on the data for single sea states and without recurved parapet. Table 7 shows the RMSE for the methods that have been developed over the last decades. From the existing methods, the one by Goda (2009) appears to be

Table 6
RMSE using the same coefficients in Eqs. (9) and (11) for bimodal wave conditions ($c_{swell} = 0.4$ is optimal).

Coefficient c in Eq. (11)	a	b	c_β	RMSE			
				$c_{swell} = 0$	$c_{swell} = 0.3$	$c_{swell} = 0.4$	$c_{swell} = 0.5$
$c = 1.0$	0.2	3.9	0.75	0.303	0.165	0.147	0.150
$c = 1.3$	0.047	2.57	0.70	0.314	0.169	0.153	0.165

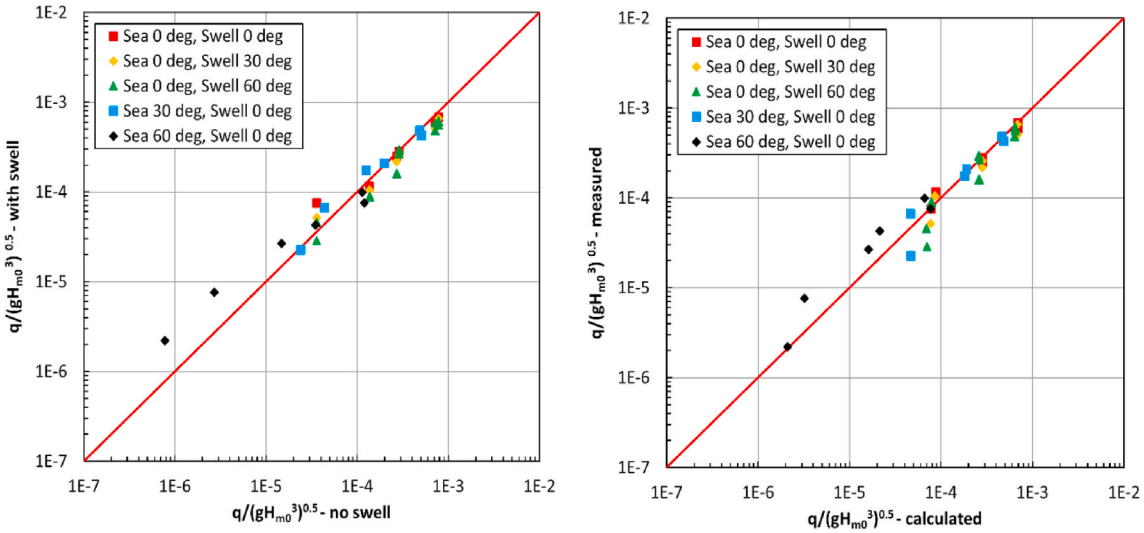

Fig. 14. Left panel: Comparison between measured overtopping discharges with and without swell; Right panel: Comparison between measured and calculated discharges for bimodal wave conditions ($a = 0.047$, $b = 2.57$, $c = 1.3$, $c_\beta = 0.70$ in Eqs. (9) and (11)).

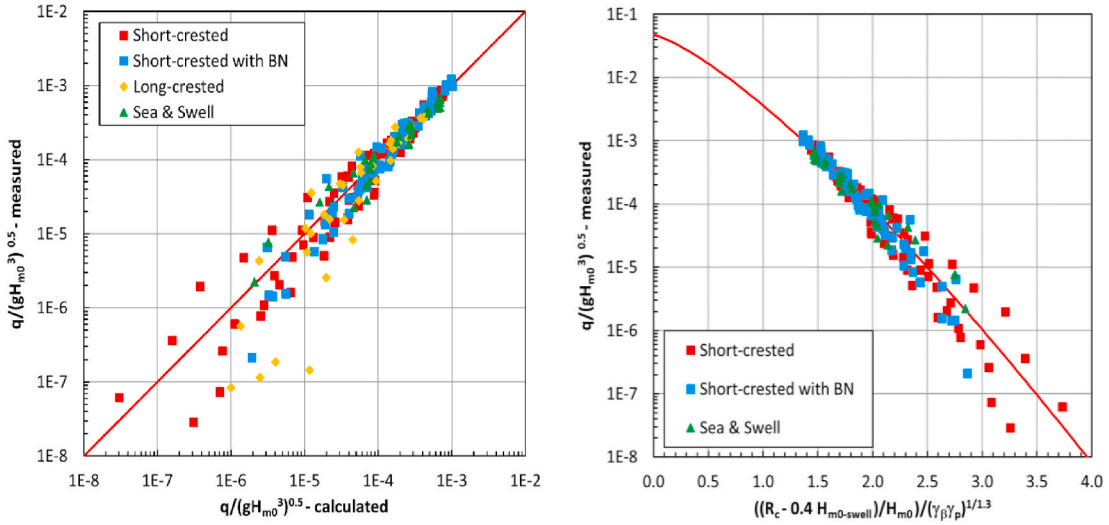

Fig. 15. Comparison between measured and calculated overtopping discharges; left panel: measured versus calculated (all data); right panel: measured versus relative crest height (all conditions with short-crested waves).

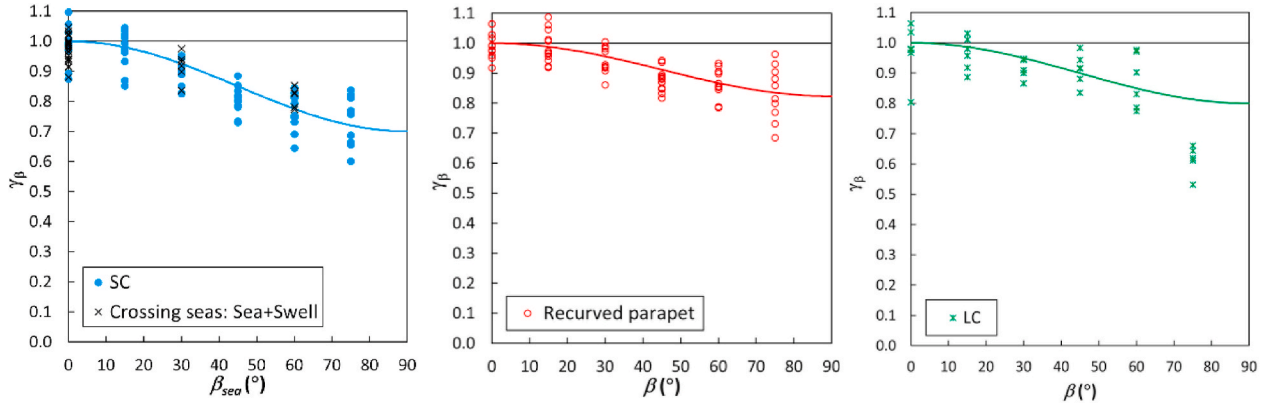

Fig. 16. Illustration of difference between measured and predicted values for (a) Short-crested waves (SC), including sea states combined with simultaneous swell, on structures without a recurved parapet, (b) Short-crested waves on structures with a recurved parapet, and (c) Long-crested waves (LC).

Table 7
Comparison between various methods for data on single sea states and without recurved parapet.

Reference	a	b	c	γ_β -LC	γ_β –SC	RMSE-LC	RMSE-SC
Franco and Franco (1999)	0.116	3.0	1.0	Eq. (2)	Eq. (3)	0.613	0.669
EM (2007)	0.04	2.6	1.0	Eq. (5)	Eq. (5)	0.451	0.388
Goda (2009)	0.027	2.3	1.0	Eq. (4)	Eq. (4)	0.447	0.352
EM (2018)	0.047	3.04	1.3	Eq. (6)	Eq. (7)	1.196	0.685
Proposed here ($c = 1$):	0.2	3.9	1.0	Eq. (10): $c_\beta = 0.80$	Eq. (10): $c_\beta = 0.75$	0.280	0.240
Proposed here ($c = 1.3$):	0.047	2.57	1.3	Eq. (10): $c_\beta = 0.80$	Eq. (10): $c_\beta = 0.70$	0.278	0.245

the most accurate one for long-crested wave and for short-crested waves while the EM2018 shows the lowest accuracy.

Note that the two proposed options (either $c = 1$ or $c = 1.3$ in Eq. (1) or Eq. (11)) lead to the lowest two values for RMSE. The differences between these two sets with $c = 1$ or $c = 1.3$ are so small that they can be considered as negligible. Note that the RMSE for structures with a recurved parapet are lower than those without recurved parapet. In the present tests the conditions with long-crested perpendicular waves lead to somewhat different discharges than those for short-crested waves. This leads to slightly different values for the coefficient b. Since the values for long-crested waves are based on only a few data-points it is advised to use the b-values obtained for short-crested waves also for long-crested waves. Nevertheless, in Table 7 the RMSE values for long-crested waves are those with modified values for b (*i.e.* 4.0 and 2.7 for long-crested waves instead of 3.9 and 2.57 for short-crested waves, for $c = 1$ and $c = 1.3$ respectively).

Of course, the relatively good performance of the proposed method is affected by the fact that the coefficients have been calibrated based on the present data-set. In contrast to earlier methods, the proposed method allows to include the combined effects of oblique waves and a recurved parapet, and it also deals with the effects of a combination of sea and swell.

5. Conclusions and recommendations

Wave overtopping at vertical breakwaters and seawalls has been studied using physical model tests in a wave basin. The influence of oblique waves on the amount of wave overtopping has been measured for caisson breakwaters with and without a recurved parapet (also referred to as a bullnose or a recurved wave return wall). The reduction in wave overtopping discharge is large for very oblique waves. The effect of a recurved parapet on the overtopping discharge can be large but reduces for larger angles of wave attack. Adding a (recurved) parapet or crown wall on top of an existing caisson breakwaters can be a solution to adapt existing caisson breakwaters to account for effects of sea level rise.

Crossing bimodal seas with simultaneous sea and swell conditions from different directions have been tested. It appears that the swell component affects the overtopping in a similar way as an increase of the water level; simultaneous swell can be accounted for by reducing the effective freeboard with a factor 0.4 times the wave height of the swell component.

Existing prediction methods have been extended and calibrated based on the present data-set. The new prediction method (*i.e.* Eq. (11) with Eq. (10) to account for oblique waves) provides estimates of overtopping discharges at trunk sections of vertical breakwaters and seawalls with or without a recurved parapet, for oblique wave attack of single sea states (*i.e.* wind waves, short-crested or long-crested) and for a combination of simultaneous wind waves and swell conditions. The influence of the recurved parapet is accounted for by incorporating an influence factor γ_p and the influence of oblique waves is accounted for by an influence factor γ_β that depends also on γ_p. At the corner section of the caisson breakwater the overtopping discharge appeared to be somewhat larger than at the trunk sections. The increase of overtopping discharges at corner sections can be accounted for by an influence factor $\gamma_{corner} = 1.05$ (for a trunk section use $\gamma_{corner} = 1$):

$$\frac{q}{\sqrt{gH_{m0}^3}} = a\ \exp\left[-\frac{b}{\gamma_\beta\ \gamma_p\ \gamma_{corner}}\left(\frac{R_c - 0.4\ H_{m0-swell}}{H_{m0}}\right)^c\right] \quad with\ \ \gamma_\beta = \left(1 - \frac{c_\beta}{\gamma_p}\right)\cos^2\beta\ +\ \frac{c_\beta}{\gamma_p} \tag{12}$$

with for short-crested waves either $a = 0.2$, $b = 3.9$, $c = 1$, $c_\beta = 0.75$ or $a = 0.047$, $b = 2.57$, $c = 1.3$, $c_\beta = 0.7$. H_{m0} is the spectral wave height of the incident waves of the wind waves (thus excluding the swell denoted by $H_{m0\text{-swell}}$). The method is valid for wave angles of $0^\circ \le \beta \le 75^\circ$ and for caisson breakwaters with freeboards of $1.2 \le R_c/H_{m0} \le 2.9$. The expressions were derived based on conditions with so-called non-impulsive wave loading with $(h/H_{m0})^2\ s_{m\text{-}1,0} > 0.25$. This corresponds to caisson breakwaters in relatively deep water, for which caisson breakwaters are often regarded as a feasible solution. Although rubble mound structures are often more feasible for less deep water, it is recommended to verify the validity of the proposed method also for caisson breakwaters in shallower water, potentially leading to impulsive loading. For impulsive wave loading also the influence of the wave period (wave steepness) should be studied.

The physical model tests showed overtopping discharges at the tip (corner) of the vertical caisson breakwater that were larger than at the trunk. It is recommended to analyse this increase at the corner in more detail, not only for a horizontal foreshore as studied here, but also for conditions with more complicated bathymetries.

To reduce wave reflection, perforated caisson breakwaters can be a suitable solution. Whether the influence of oblique waves on the reduction in wave overtopping for perforated caisson breakwaters is similar to the influence for unperforated caisson breakwaters, could be a topic for future research. Use can be made of initial data and insights by Franco and Franco (1999) with respect to wave overtopping at perforated caissons under oblique waves.

The present study is based on tests with a caisson breakwater with and without a recurved parapet. The shape of the parapet has not been varied in the present study. It is recommended to verify the validity of the derived expressions to account for oblique wave attack also for other geometries of the parapet.

Author statement

MvG: Conceptualization, Methodology, Investigation, Formal analysis, Writing- Original draft and editing.

Declaration of competing interest

The authors declare that they have no known competing financial interests or personal relationships that could have appeared to influence the work reported in this paper.

Acknowledgements

The assistance by my colleagues Mr. Wesley Stet (during the actual model tests), Mr. Ivo van der Werf and Dr. Guido Wolters (review of this article) is highly appreciated.

References

Battjes, J.A., 1974. Computation of Set-Up, Longshore Currents, Run-Up and Overtopping Due to Wind-Generated Waves.. Ph.D.-thesis TU Delft.
Castellino, M., Sammarco, P., Romano, A., Martinelli, L., Ruol, P., Franco, L., De Girolamo, P., 2018. Large impulsive forces on recurved parapets under non-breaking waves. A numerical study. Coast. Eng. 136, 1–15.

Den Bieman, J.P., Wilms, J.M., van den Boogaard, H.F.P., van Gent, M.R.A., 2020. Prediction of mean wave overtopping discharge using gradient boosting decision trees. MDPI Water 12 (6), 1703. https://doi.org/10.3390/w12061703, 2020.
manual, E.A., 1999. Overtopping of Seawalls – Design and Assessment Manual, R & D Technical Report W 178. Environment Agency, Bristol.
EurOtop manual, 2007. Wave overtopping of sea defences and related structures–assessment manual. In: Allsop, N.W.H., Pullen, T., Bruce, T., van der Meer, J.W., Schüttrumpf, H., Kortenhaus, A. (Eds.). www:overtopping-manual.com.
EurOtop manual, 2018. Manual on wave overtopping of sea defences and related structures. In: van der Meer, J.W., Allsop, N.W.H., Bruce, T., de Rouck, J., Kortenhaus, A., Pullen, T., Schüttrumpf, H., Troch, P., Zanuttigh, B. (Eds.). www.overtopping-manual.Com (incl. Errata November 2019.
Franco, C., Franco, L., 1999. Overtopping formulas for caisson breakwaters with nonbreaking 3D waves. J. Waterw. Port, Coast. Ocean Eng. 125, 98–108.
Franco, L., de Gerloni, M., van der Meer, J.W., 1994. Wave overtopping on vertical and composite breakwaters. In: ASCE, Proc. ICCE 1994, pp. 1030–1045.
Franco, L., de Gerloni, M., Passoni, G., Zacconi, D., 1998. Wave forces on solid and perforated caisson breakwaters: comparison of field and laboratory measurements. In: Proc. ICCE 1998, pp. 1945–1958 (Copenhagen).
Goda, Y., 1971. Expected rate of irregular wave overtopping of seawalls. Coast. Eng. Jpn. 14, 45–51 (JSCE, Tokyo).
Goda, Y., 1974. A new method of wave pressure calculation for the design of composite breakwaters. In: Proc. ICCE 1974, pp. 1702–1720 (Copenhagen).
Goda, Y., 1985. Random Seas and Design of Maritime Structures. University of Tokyo Press, Tokyo (1985); Third edition: World Scientific (2010).
Goda, Y., 2009. Derivation of unified wave overtopping formulas for seawalls with smooth, impermeable surfaces based on selected CLASH datasets. Coast. Eng. 56, 385–399, 2009.
Ito, M., Tanimoto, K., 1971. Meandering Damages of Composite Type Breakwaters. Report Port and Harbour Research Institute, No, p. 112 (in Japanese).
Kortenhaus, A., Pearson, J., Bruce, T., Allsop, N., van der Meer, J., 2003. Influence of parapets and recurves on wave overtopping and wave loading of complex vertical walls. Proc. Coast. Struct. 369–381 (Portland, USA).
Martinelli, L., Ruol, P., Volpato, M., Favaretto, C., Castellino, M., de Girolamo, P., Franco, L., Romano, A., Sammarco, P., 2018. Experimental investigation on non-breaking wave forces and overtopping at the recurved parapets of vertical breakwaters. Coast. Eng. 141, 52–67.
Mase, H., Memita, T., Yuhi, M., Kitano, T., 2002. Stem waves along vertical wall due to random wave incidence. Coast. Eng. 44, 339–350.
Napp, N., Bruce, T., Pearson, J., Allsop, W., 2004. Violent Overtopping of Vertical Seawalls under Oblique Wave Conditions. Proc. ICCE 2004, Lisbon.
Owen, M.W., 1980. Design of Sea Walls Allowing for Wave Overtopping. Report EX 924, HR Wallingford.
Pearson, J., Bruce, T., Allsop, W., Kortenhaus, A., van der Meer, J., 2004. Effectiveness of recurve walls in reducing wave overtopping on seawalls and breakwaters. In: Proc. ICCE 2004, pp. 4404–4416 (Lisbon).
Petrova, P.G., Guedes Soares, C., 2014. Distributions of nonlinear wave amplitudes and heights from laboratory generated following and crossing bimodal seas. Nat. Hazards Earth Syst. Sci. 14, 1207–1222, 2014.
Petrova, P.G., Tayfun, M.A., Guesdes Soares, C., 2013. The effect of third-order nonlinearities on the statistical distributions of wave heights, crests and troughs in bimodal crossing seas. J. Offshore Mech. Arctic Eng. 135, 2013.
Tabet-Aoul, E.H., Lambert, E., 2003. Tentative new formula for maximum horizontal wave forces acting on perforated caisson. J. Waterway Port Coast. Ocean Eng. ASCE 129, 34–40.
Takahashi, S., 1996. Design of Vertical Breakwaters, Reference Document N34. Port and Harbour Research Institute, Japan. https://doi.org/10.1142/9789814282413_0004 revised July 2002.
Takahashi, S., Kotake, Y., Fujiwra, R., Isobe, R.M., 2002. Performance evaluation of perforated-wall caissons by VOF numerical simulations. In: Proc. ICCE 2002, pp. 1364–1376 (Cardiff).
Van der Werf, I.M., van Gent, M.R.A., 2018. Wave overtopping over coastal structures with oblique wind and swell waves. J. Mar. Sci. Eng. 6 (4), 149. https://doi.org/10.3390/jmse6040149, 2018.
Van Gent, M.R.A., 2014. Oblique wave attack on rubble mound breakwaters. Coast. Eng. 88, 43–54. https://doi.org/10.1016/j.coastaleng.2014.02.002.
Van Gent, M.R.A., 2020. Influence of oblique wave attack on wave overtopping at smooth and rough dikes with a berm. Coast. Eng. 160 https://doi.org/10.1016/j.coastaleng.2020.103734.
Van Gent, M.R.A., van den Boogaard, H.F.P., 1998. Neural Network Modelling of Forces on Vertical Structures, ASCE. Proc. ICCE 1998, Copenhagen.
Van Gent, M.R.A., van der Werf, I.M., 2019. Influence of oblique wave attack on wave overtopping and wave forces on rubble mound breakwater crest walls. Coast. Eng. 151, 78–96. https://doi.org/10.1016/j.coastaleng.2019.04.001.
Van Gent, M.R.A., van den Boogaard, H.F.P., Pozueta, B., Medina, J.R., 2007. Neural network modelling of wave overtopping at coastal structures. Coast. Eng. 54, 586–593.
Vieira Leite, J.P., van der Meer, J.W., Franco, L., Romano, A., Pepi, Y., Bruce, T., Vieira Pinheiro, L., Menendez, M., 2019. Distribution of overtopping wave volumes caused by crossing seas. Proc. Coast. Struct. https://doi.org/10.18451/978-3-939230-64-9_113, 2019, Hannover.
Wenneker, I., Meesters, J., Hoffmann, R., Francissen, D., 2010. Active Wave Absorption System ARCH, Proc. 3rd International Conference on the Application of Physical Modelling to Port and Coastal Protection (Barcelona, Spain).

Glossary

α_E: exit angle of a recurved parapet [°]
β: angle of wave attack of wind waves: $\beta = \beta$sea [°]
β*swell:* angle of wave attack of swell [°]
γ: influence factor [−]
γ*corner:* influence factor for a corner section compared to a trunk section [−]
γp: influence factor for a parapet [−]
γ*#:* influence factor for crossing seas [−]
$\gamma\beta$: influence factor for the angle of wave attack [−]
σ: directional spreading (normal distribution) [°]
Br: protruding part of a (recurved) parapet [m]
g: acceleration due to gravity [m/s2]
Hm0: significant wave height of the incident waves based on the wave energy spectrum [m]
h: water depth [m]
k: ratio between overtopping discharges with and without a parapet [−]
N: number of waves [−]
Q: non-dimensional mean overtopping discharge: Q = q /(gHm03)0.5 [-]
q: mean overtopping discharge [m3/s/m]
Rc: freeboard (crest height relative to the still water level) [m]
R: radius of a recurved parapet [m]
sm-1,0: wave steepness based on the wave height Hm0 and the spectral wave period Tm-1,0: sm-1,0 = 2π Hm0 / gTm-1,02[-]
Tm-1,0: spectral mean wave period based on the ratio of the spectral moments m_{-1} and m_0 of the incident wave spectrum [s]